J. Fluid Mech. (2000), *vol.* 412, *pp.* 1–20. Printed in the United Kingdom

Scaling and parameterization of stratified homogeneous turbulent shear flow

By LUCINDA H. SHIH[1], JEFFREY R. KOSEFF[1], JOEL H. FERZIGER[1] AND CHRIS R. REHMANN[2]

[1]Environmental Fluid Mechanics Laboratory, Department of Civil and Environmental Engineering, Stanford University, Stanford, CA 94305, USA

[2]Hydrosystems Laboratory, Department of Civil and Environmental Engineering, University of Illinois at Urbana-Champaign, Urbana, IL 61801, USA

(Received 5 September 1998 and in revised form 1 August 1999)

Homogeneous sheared stratified turbulence was simulated using a DNS code. The initial turbulent Reynolds numbers (Re) were 22, 44, and 89, and the initial dimensionless shear rate (S^*) varied from 2 to 16. We found (similarly to Rogers (1986) for unstratified flows) the final value of S^* at high Re to be ~ 11, independent of initial S^*. The final S^* varies at low Re, in agreement with Jacobitz *et al.* (1997). At low Re, the stationary Richardson number (Ri_s) depends on both Re and S^*, but at higher Re, it varies only with Re. A scaling based on the turbulent kinetic energy equation which suggests this result employs instantaneous rather than initial values of flow parameters.

At high Re the dissipation increases with applied shear, allowing a constant final S^*. The increased dissipation occurs primarily at high wavenumbers due to the stretching of eddies by stronger shear. For the high-Re stationary flows, the turbulent Froude number (Fr_t) is a constant independent of S^*. An Fr_t-based scaling predicts the final value of S^* well over a range of Re. Therefore Fr_t is a more appropriate parameter for describing the state of developed stratified turbulence than the gradient Richardson number.

1. Introduction

Homogeneous turbulence subjected to shear and stratification is the simplest type of flow in which many of the major phenomena found in geophysical turbulence occur. Thus, it is hardly surprising that it has been the subject of a number of investigations both experimental and numerical. Since the applications of this flow are listed and described in the papers referenced below, we shall not present them here.

The first numerical investigation of this type of flow was made by Gerz, Schumann & Elghobashi (1989). They established the major effects of adding stratification to a turbulent shear flow, namely that turbulence energy grows when the stratification is weak and decays when the stratification is strong. Webster (1964) conducted early experiments on stratified shear flow in a wind tunnel, observing that turbulence structures vary with the gradient Richardson number of the flow. There have been numerous laboratory studies of homogeneous stratified turbulence, many of which are discussed in Rohr *et al.* (1988) and Piccirillo & Van Atta (1997). Rohr *et al.* (1988) conducted experiments which added shear to homogeneous stably stratified

turbulence; their results indicated that the growth of turbulent kinetic energy is supressed at a Richardson number of 0.25 ± 0.05. Gerz *et al.* (1989) and Holt, Koseff & Ferziger (1992, hereinafter referred to as HKF) were the first to employ direct numerical simulations (DNS) of sheared, stratified flow. In particular, HKF demonstrated the existence of a stationary Richardson number Ri_s and its dependence on the Reynolds number, presenting data suggesting that its value is independent of the initial dimensionless shear rate.

Piccirillo & Van Atta (1997) also performed laboratory experiments on homogeneous stratified shear flow. Their findings prompted Jacobitz, Sarkar & Van Atta (1997, hereinafter referred to as JSV) to perform further numerical investigations and to propose that in sheared and stratified homogeneous turbulence, the stationary Richardson number depends on both the Reynolds number and the initial dimensionless shear rate of the flow. If correct, this scenario necessitates a more complex description of turbulence subjected to shear and stratification and suggests that modelling of flows in which these forcings both occur might be difficult. The apparent discrepancy between the findings of the HKF and JSV studies motivates further inquiry into the dependence of the flow state on its initial conditions. Specifically, we are led to ask whether the stationary Richardson number of stratified, sheared flow depends on the initial dimensionless shear rate, and, if it does, what the conditions of dependence are.

The gradient Richardson number Ri, which is commonly used to correlate turbulence data in stratified shear flows (including those simulated in the above-referenced studies), is a global parameter that depends on the imposed conditions rather than on the local instantaneous state of the turbulence. Ivey & Imberger (1991), among others, proposed a turbulent Froude number Fr_t based on the local properties of the turbulence as a viable parameter for characterizing the turbulence of stratified shear flows. Kaltenbach, Gerz & Schumann (1994) discovered that in sheared turbulent flow with very strong stratification ($Ri > Ri_s$), an inverse Froude number serves well as a proxy for the independent time variable to collapse data from simulations performed over a range of Ri. They asserted that an examination of the Froude number would serve to explain the apparent Reynolds number dependence on Ri_t, the transition Richardson number defined by HKF to mark the change from shear-dominated to buoyancy-dominated flows.

Garg (1996) found that, in stratified channel flow, the gradient Richardson number varies by two orders of magnitude across the channel and is not useful for characterizing the buoyancy effects on the turbulence. Near the channel boundary, where Ri is very low, the turbulence is suppressed, counter to what one would expect where the gradient Richardson number indicates minimal stratification; furthermore, in the channel core turbulence was found to be still active despite a large Ri. However, Garg did also find that the local turbulent Froude number did an excellent job of correlating the turbulence data in all regions of the flow. Briggs *et al.* (1998) also found Fr_t to do well in characterizing many features of shear-free stratified turbulence. This evidence prompts us to revisit data on homogeneous stratified sheared turbulence to ask whether it might be better correlated with the turbulent Froude number.

To answer the questions posed above, we have performed a series of direct numerical simulations over a range of initial Reynolds numbers (Re) and dimensionless shear rates (S^*). These simulations cover the same range of S^* used by JSV and, in addition, extend the Re range. We use the same initial spectrum as JSV with the goal of reproducing their results for the low-Re simulations, and, thereby, establishing a sound base for comparison. We first investigate the behaviour of the dimensionless

shear rate over a wider range of Reynolds numbers than the relatively low values used in JSV, and we also examine the dependence of the stationary Richardson number on both of these quantities. In addition, we examine the data generated by the simulations and employ scaling arguments which suggest the best set of parameters for correlating the results. Finally, we present some useful correlations for interpreting the data and employing the results in modelling flows of this type.

2. The simulations

2.1. *The flow*

The simulated flow is homogeneous stably stratified turbulent flow subjected to constant shear. The governing equations are the conservation-of-mass equation for an incompressible fluid, the Boussinesq form of the Navier–Stokes equations, and an equation for the transport of density, and are

$$U_{i,i} = 0, \tag{1}$$

$$U_{i,t} + U_j U_{i,j} = -\frac{1}{\rho_0} P_{,i} - \frac{g}{\rho_0}\rho\delta_{i3} + \nu U_{i,jj}, \tag{2}$$

$$\varrho_{,t} + U_j \varrho_{,j} = \gamma \varrho_{,jj}\,, \tag{3}$$

with velocity $U_i = \bar{U}_i + u_i$, where $\bar{U}_i$ is the mean velocity and u_i is the fluctuating velocity, and density $\varrho = \bar{\rho} + \rho$, where $\bar{\rho}$ is the mean density and ρ is the fluctuating density, ν is the kinematic viscosity, and γ is the diffusivity. Mean density is defined as $\bar{\rho} = \rho_0 + S_\rho x_3$, where ρ_0 is a constant reference density, S_ρ is the mean density gradient, and x_3 is the vertical coordinate. Uniform shear flow is introduced by setting the mean velocity $\bar{U}_i = (Sx_3, 0, 0)$, where S is the imposed mean shear rate. Also, $(x_1, x_2, x_3) = (x, y, z)$ and $(u_1, u_2, u_3) = (u, v, w)$ are used interchangeably.

The numerical method used in this investigation is summarized in HKF, with more complete details given in Holt (1990). The code solves the above equations with second-order Runge–Kutta time advancement and periodic boundary conditions for all of the turbulent quantities. It is based on the pseudospectral method developed by Rogallo (1981). As described in Holt (1990) and Rogallo (1981), masking and random phase shifting are employed to remove aliasing error, resulting in a residual aliasing error of the same order as the error due to the time advancement scheme. We believe that the accuracy of this code and its dealiasing technique has been amply demonstrated in HKF and therefore shall not present further validation cases here.

2.2. *Initial conditions*

Chosen initial values of the dimensionless numbers S^*, Re_λ, and Ri are used to set the flow conditions. The dimensionless shear rate S^* is defined as

$$S^* = \frac{Sq^2}{\epsilon}, \tag{4}$$

where $S = \mathrm{d}U/\mathrm{d}z$ is the mean shear rate, $K = q^2/2$ is the turbulent kinetic energy, and ϵ is the rate of dissipation of the turbulent kinetic energy. The turbulent Reynolds number is defined as

$$Re_\lambda = \frac{q\lambda}{\nu}, \tag{5}$$

where λ is the Taylor microscale. The initial values of Re_λ, S^* and Ri are varied from run to run, as enumerated in table 1. The strength of the stratification is indicated by

Run	$Re_{\lambda,initial}$	S_0^*	Ri
pa	22.36	2	0.06
pc	22.36	4	0.06
pb	22.36	8	0.06
pe	22.36	16	0.06
ga	44.72	2	0.16
gc	44.72	4	0.16
gb	44.72	8	0.16
gd	44.72	16	0.16
fz	89.44	2	0.16
fc	89.44	4	0.16
fb	89.44	8	0.16
fd	89.44	16	0.16

TABLE 1. Initial conditions for k^2-exponential initial energy spectrum runs.

the gradient Richardson number

$$Ri = \frac{N^2}{S^2}, \tag{6}$$

where $N = -(g/\rho)(\partial\bar{\rho}/\partial z)^{1/2}$ is the Brunt–Väisälä frequency; Ri is constant in each simulation. Other parameters, which were not varied in this study are the Schmidt number $Sc = \nu/\gamma = 0.72$, gravitational acceleration $g = 980.7\,\mathrm{cm\,s^{-2}}$, and reference density $\rho_0 = 1.006\,\mathrm{g\,cm^{-3}}$. The value of the Schmidt number matches that used by JSV and was chosen so that direct comparisons of results could be made. The domain for all of the simulations, save the one exception mentioned below, was sub-divided into a $128 \times 128 \times 128$ grid, with coordinate stretching factors $\beta_1 = 2^{-2/3}$ and $\beta_2 = \beta_3 = 2^{1/3}$ to allow for the shear-induced growth of the integral scales in the streamwise direction (Rogallo 1981).

The results from a single high-Reynolds-number simulation with a grid of 256^3 points confirm that a 128^3 grid is adequate for the purposes of this study. There exist slight quantitative differences between the two cases, but there is no indication that increasing the resolution of the domain alters the qualitative accuracy of the findings presented below from the 128^3 grid simulations. The energy spectra evolve very similarly, as shown in figure 1(*a*). The dissipation spectra in figure 1(*b*) show that, as expected, the finer grid yields slightly more dissipation, since more of the small scales are resolved. This increase in dissipation for the 256^3 grid case reduces the total turbulent kinetic energy relative to the less-dissipative 128^3 grid case by the small amount visible in figure 1(*c*). This simulation is a stationary case (see below for details) for the 128^3 grid, but the increased dissipation at higher resolution makes the turbulence decay slightly. Thus the stationary Richardson number for the 256^3 grid is expected to be uniformly reduced by a small amount compared to that for the coarser grid. All of the results presented in this paper were obtained using the 128^3 grid.

Two different initial energy spectra were used in this study. The 'top hat' or square-pulse spectrum, used by HKF, is defined by

$$E(k) = \begin{cases} e_0 & \text{for} \quad k_0 < k < k_c \\ 0 & \text{otherwise,} \end{cases} \tag{7}$$

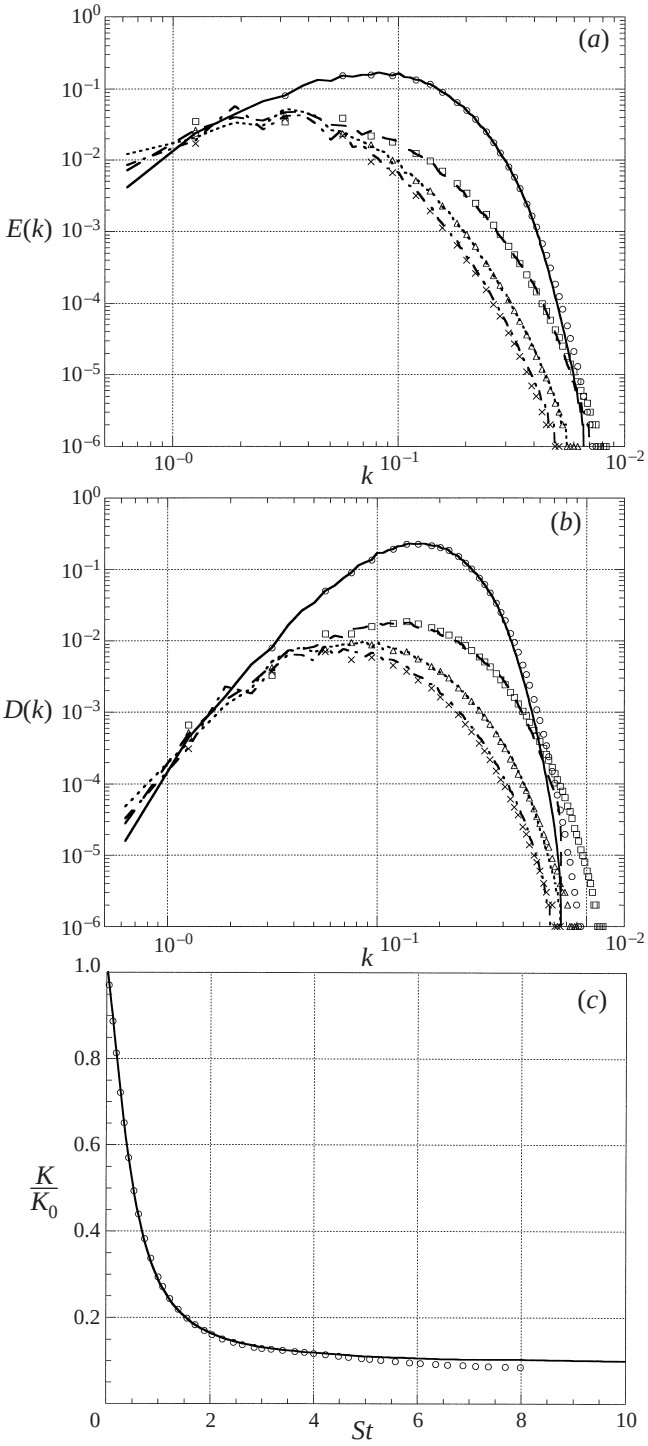

FIGURE 1. Comparison of results from simulations using a 128^3 grid and a 256^3 grid. $Re_{\lambda,initial} = 89.44$, $Ri = 0.16$, $S_0^* = 2$. Evolution of (*a*) the energy and (*b*) the dissipation spectra over non-dimensional time St. 128^3 grid: —, $St = 0$; – –, $St = 2$; · · · · ·, $St = 4$; · — ·, $St = 8$; 256^3 grid: ○, $St = 0$; □, $St = 2$; △, $St = 4$; ×, $St = 8$; (*c*) Evolution of normalized turbulent kinetic energy: —, 128^3 grid; ○, 256^3 grid.

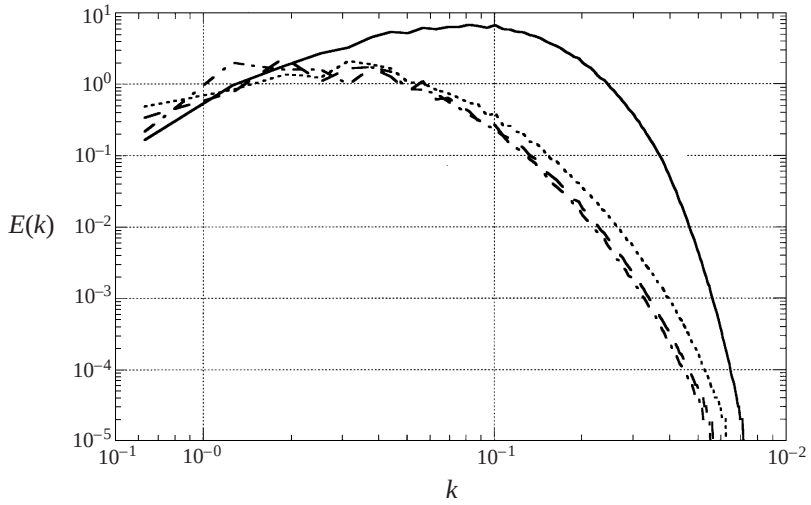

FIGURE 2. Evolution of the energy spectrum from a k^2-exponential initial energy spectrum. $Re_{\lambda,initial} = 89.44$, $Ri = 0.16$, $S_0^* = 2$. —, $St = 0$; · · · · ·, $St = 4$; – –, $St = 8$; · — ·, $St = 12$.

where e_0 is a constant, k is wavenumber, and k_0 and k_c specify the width of the pulse. The k^2-exponential spectrum, proposed by JSV, is defined as

$$E(k) = A\left(\frac{k}{k_p}\right)^2 \mathrm{e}^{-2k/k_p}, \tag{8}$$

where A is a constant and k_p is the wavenumber at the peak of the spectrum. The results of simulations using both initial energy spectra are qualitatively similar. Figure 2 shows how the energy evolves from a k^2-exponential initial energy spectrum in a typical case.

JSV initialized their shear flow simulations with information from simulations of isotropic turbulence developed for one eddy-turnover time. They found that the k^2-exponential spectrum closely resembled their initial spectrum and thus deemed it to be more physically reasonable than other initialization options used in previous studies. Since the top-hat initialization introduces energy within a limited range of wavenumbers, the initial stage of a simulation using this spectrum is characterized by a redistribution of energy to all of the energy-containing scales. The k^2-exponential spectrum is preferred because it allocates the initial energy across a broader range of wavenumbers. Consequently, unless otherwise specified, the data used in this paper are computed from a k^2-exponential initial energy spectrum. The results using this spectrum are very similar to those of JSV. For example, in figure 3(*a–d*) we show some of the results from our low-Reynolds number ($Re_{\lambda,initial} = 22.36$) simulations; they are essentially identical to those of JSV. Our simulations are only run to a non-dimensional time of $St = 12$ because at longer times the length scales become comparable to the domain size and the validity of the results is called into question. The jagged features apparent especially in the highest shear cases are due to the remeshing of the grid that occurs at intervals of two non-dimensional time units, starting from $St = 1$. Remeshing is necessary to prevent the shearing grid from distorting to useless proportions.

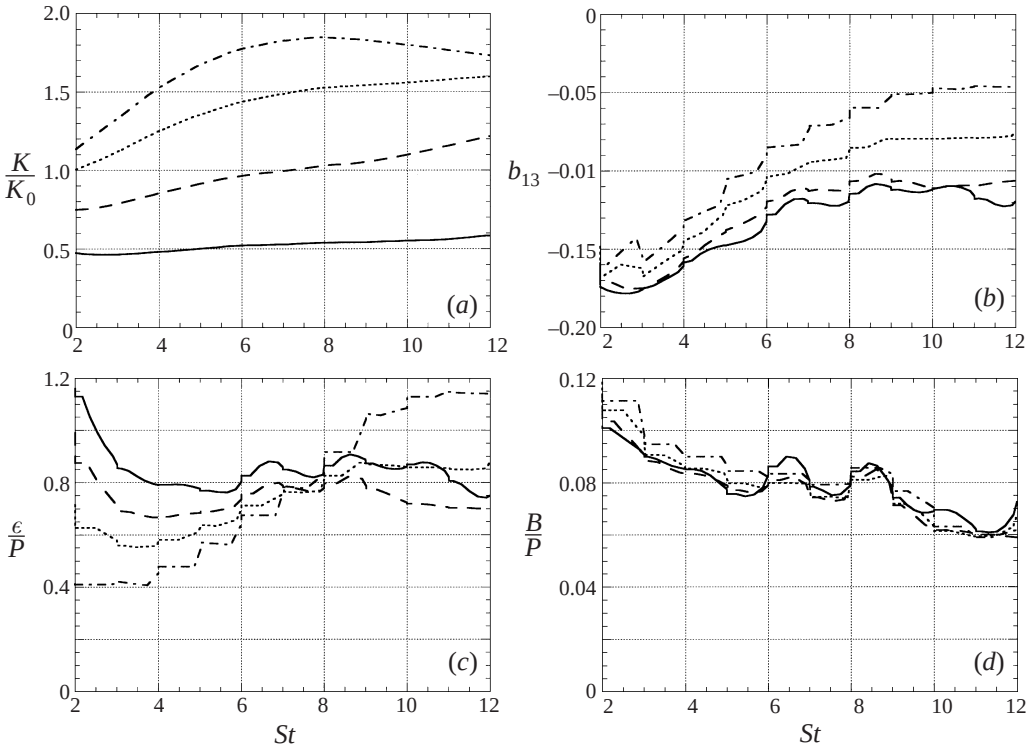

FIGURE 3. Evolution of selected turbulence statistics: (*a*) the turbulent kinetic energy K, normalized by the initial kinetic energy K_0; (*b*) the 1, 3 component of the velocity anisotropy tensor b_{13}; (*c*) the ratio of dissipation ϵ to production P; and (*d*) the ratio of buoyancy B to production P, for $Re_{\lambda,initial} = 22.36$, $Ri = 0.06$ and a range of initial dimensionless shear numbers S_0^*. The data before $St = 2$ are omitted for clarity. —, $S_0^* = 2$; – –, $S_0^* = 4$; · · · · ·, $S_0^* = 8$; · — ·, $S_0^* = 16$.

3. Behaviour of the dimensionless shear rate S^*

Rogallo (1981) used dimensional analysis to postulate that the non-dimensional shear rate must approach a finite non-zero constant when time becomes large. Speziale & Mac Giolla Mhuiris (1989) also formulated an equilibrium solution to the turbulent kinetic energy equation which indicates that, in the limit of non-dimensional time going to infinity, the non-dimensional shear rate equals a constant which depends solely on K–ϵ turbulence model parameters. Rogers (1986) examined unstratified sheared homogeneous flows and found that at high Re, S^* did in fact tend to a constant, with a value around 11. This result has proven useful in the modelling of shear flows (see Speziale, Gatski & Sarkar 1992). We might, therefore, expect a similar result for stratified flows. Using the relationship for production $P = -\overline{uw}S$, S^* can be rewritten as

$$S^* = -\frac{P}{\epsilon}\left(\frac{q^2}{\overline{uw}}\right). \tag{9}$$

Figures 4(*a*) and 4(*b*) show that at high Re, $q^2/\overline{uw}(= 1/b_{13})$ tends to a constant independent of initial conditions, and at equilibrium $P \sim \epsilon$. Therefore, equation (9) shows that S^* approaches a constant $-q^2/\overline{uw}$.

Figure 5(*a–c*) illustrates the time evolution of S^* for the initial conditions listed in table 1. For low initial $Re_\lambda = 22.36$ (figure 5*a*), S^* grows continually from its initial

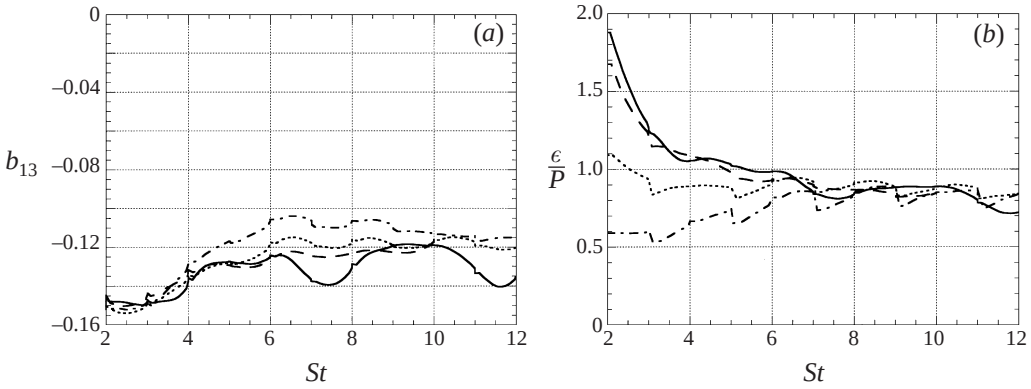

FIGURE 4. Evolution of (*a*) the 1, 3 component of the velocity anisotropy tensor and (*b*) the ratio of dissipation to production for $Re_{\lambda,initial} = 89.44$, $Ri = 0.16$, and a range of S_0^*. The data before $St = 2$ are omitted for clarity. —, $S_0^* = 2$; – –, $S_0^* = 4$; · · · · ·, $S_0^* = 8$; · — ·, $S_0^* = 16$.

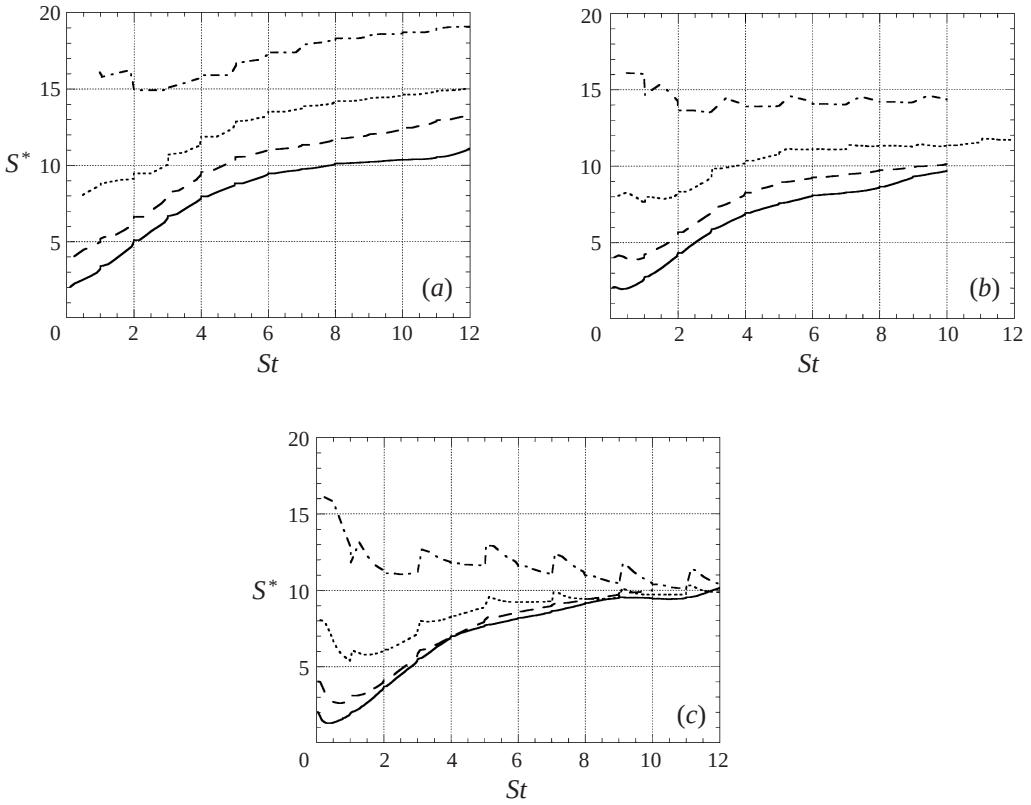

FIGURE 5. Evolution of S^* for (*a*) $Re_{\lambda,initial} = 22.36$, $Ri = 0.06$, (*b*) $Re_{\lambda,initial} = 44.72$, $Ri = 0.16$, and (*c*) $Re_{\lambda,initial} = 89.44$, $Ri = 0.16$. —, $S_0^* = 2$; – –, $S_0^* = 4$; · · · · ·, $S_0^* = 8$; · — ·, $S_0^* = 16$.

value, and the value of S^* at large time is clearly dependent on its initial value. This result agrees with the findings of JSV. For high initial $Re_\lambda = 89.44$ (figure 5*c*) however, the value of S^* converges to a constant value of approximately 10.5, independent of its initial value. For intermediate initial $Re_\lambda = 44.72$ (figure 5*b*), S^* shows a

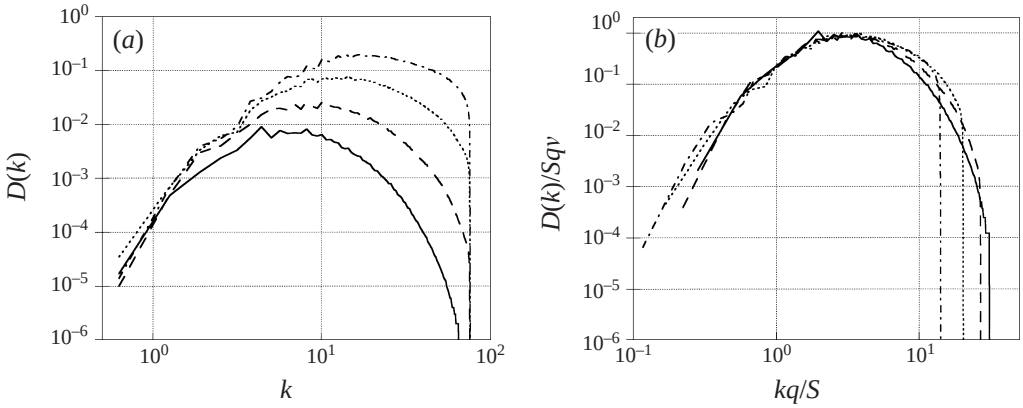

FIGURE 6. Dissipation spectra at $St = 10$ for various initial dimensionless shear rates. $Re_{\lambda,initial} = 89.44, Ri = 0.16$: (*a*) unnormalized, where $D(k)$ is in units of $cm^3\ s^{-3}$ and k is in units of cm^{-1}, and (*b*) normalized. —, $S_0^* = 2$; – –, $S_0^* = 4$; · · · ·, $S_0^* = 8$; · — ·, $S_0^* = 16$.

tendency to converge to the same constant value as in the high-Reynolds-number cases, but the convergence is slower. The Reynolds number effect on S^* evolution is the same for both the top-hat and k^2-exponential initial energy spectra, and for both high ($Ri = 0.16$) and low ($Ri = 0.06$) levels of stratification. We conclude that, at high Reynolds number, S^* tends to a unique value independent of the initial S^*, consistent with the hypothesis of Rogallo (1981) and the findings of Rogers (1986) for unstratified flow.

Given that $S^* = Sq^2/\epsilon$ evolves to a constant value in the high initial Reynolds number runs regardless of the initial value of S^* and the shear rate S is a constant in each run, it seems prudent to investigate the behaviour of the turbulent kinetic energy $K = q^2/2$ and dissipation ϵ. The initial kinetic energy and the initial dissipation are fixed in each run. The kinetic energy increases more rapidly with increasing shear, as does the dissipation. However, the ratio of kinetic energy to dissipation decreases with increasing shear, which means that the dissipation increases faster than the kinetic energy as the shear rate increases. The dissipation spectra (figure 6*a*) show that, as expected, the increase in dissipation occurs in the high wavenumbers.

A possible physical interpretation of the increased dissipation in the small scales is that stronger shear, with all other parameters held equal, stretches the eddies more. Lee, Kim & Moin (1990) observed the development of 'streaky' structures in the turbulent velocity fields, at very high shear ($S^* \approx 30$) using both DNS and rapid distortion theory (RDT) analyses of homogeneous turbulent flow. These structures are elongated in the flow direction and narrow in the spanwise direction. The longer, thinner eddies are more susceptible to breaking up, becoming even smaller eddies whose energy is more easily dissipated, thus producing the increased dissipation at the smallest scales. If the increasing shear rate fully explains the increased dissipation, we expect that normalizing the dissipation spectra by the shear rate should collapse the spectra. Non-dimensionalizing the dissipation spectra $D(k)$ by Sqv and the wavenumber k by an appropriate shear length scale q/S in figure 6(*b*), we see that the spectra do indeed collapse fairly well. From this evidence, it seems clear that the increase in the dissipation balances the increase in the production of turbulent kinetic energy, in such a way that the final value of S^* is always the same.

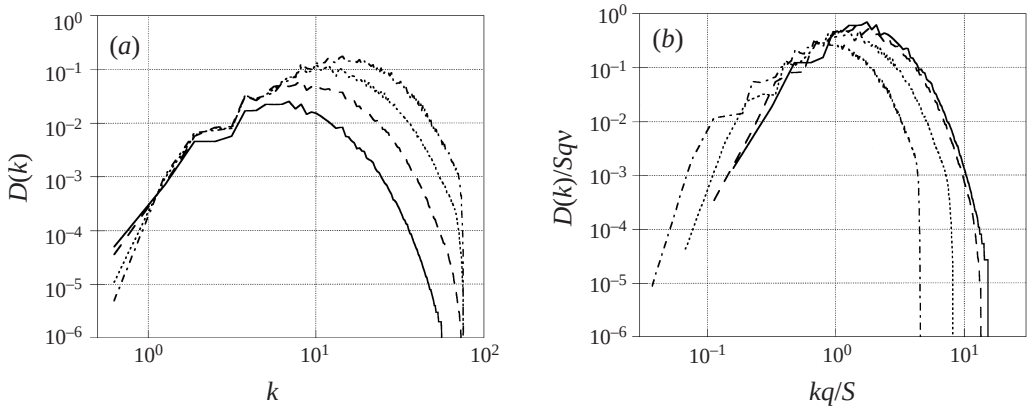

FIGURE 7. As figure 6 but at $Re_{\lambda,initial} = 22.36$, $Ri = 0.06$.

For the low-Reynolds-number case, the dissipation spectra (figure 7*a*), the evolution of turbulent kinetic energy and dissipation, and the ratio of kinetic energy to dissipation all share the trends observed in the high initial Reynolds number cases in which S^* evolves to a constant value. The high-resolution case mentioned in § 2.2 also evolves to the same values of S^*, indicating that this value does not depend on the resolution of the domain. However, when the dissipation spectra are non-dimensionalized (figure 7*b*), the curves do not collapse as well as in the high-*Re* case, hinting that, at low Reynolds number, the increased dissipation is not completely due to the increased shear, nor is the increased production completely offset by the increased dissipation. A possible explanation is that at low Reynolds number, nonlinear effects are small, so the energy transfer is also small. Energy transfer is also inhibited by both shear and stratification. The stretching of the eddies induced by the shear may also be partially offset by viscous diffusion. The similarity of the low-wavenumber regions of the dissipation spectra for the various shear rates in figure 7(*a*) is evidence supporting this reasoning.

Since the final value of S^* is independent of initial conditions at high Reynolds number, we conclude that it is not useful to characterize a flow by its initial S^*. Turbulence 'forgets' its history in about one eddy turnover time, so developed flows are dependent on their initial conditions only indirectly. Although the initial values of the parameters are useful as an overall indicator of what may be expected in a simulation, they should not be used to correlate the results. Instead, our findings suggest that instantaneous quantities are better suited to correlating the data.

It should be noted that the simulations were not able to resolve the very high wavenumbers accurately, as evidenced by the sharp cutoff in the spectra at $k \approx 80$. The higher shear cases have more of their spectra cut off than the lower shear cases, because the former extend to smaller scales than the latter. This incomplete resolution manifests itself in the dimensionless spectra as an apparent decrease in total dissipation resulting from the leftward shift of the high-wavenumber parts of the spectra. However, since the spectra do not have cusps which are characteristic of aliasing problems, it appears that the limited resolution does not interfere with the validity of our results. The dealiasing measures employed ensure that, although the energy at the highest wavenumbers is lost, the information at the remaining wavenumbers is essentially uncontaminated.

Run	$Re_{\lambda,initial}$	S_0^*	Initial energy spectrum	Ri_s	Symbol
pg	22.36	4	k^2-exponential	0.09	○
ph	22.36	12	k^2-exponential	0.06	○
pi	33.54	4	k^2-exponential	0.12	⊙
gh	44.72	2	k^2-exponential	0.14	□
dd	44.72	4	k^2-exponential	0.14	□
cd	44.72	4	top hat, $k_0 = 16$, $k_c = 32$	0.09	◇
ed	44.72	4	top hat, $k_0 = 0.25$, $k_c = 10$	0.15	◇
gn	44.72	8	k^2-exponential	0.15	□
gs	44.72	12	k^2-exponential	0.15	□
pj	67.08	4	k^2-exponential	0.15	●
fz	89.44	2	k^2-exponential	0.16	△
fc	89.44	4	k^2-exponential	0.16	△
bd	89.44	4	top hat, $k_0 = 16$, $k_c = 32$	0.12	▽
bi	89.44	4	top hat, $k_0 = 0.25$, $k_c = 10$	0.19	▽
nr	89.44	4	top hat, $k_0 = 1$, $k_c = 16$	0.18	▽
fb	89.44	8	k^2-exponential	0.16	△
nz	89.44	8	top hat, $k_0 = 1$, $k_c = 16$	0.19	▽
bx	89.44	12	k^2-exponential	0.17	△

TABLE 2. Initial conditions for the stationary turbulence runs.

4. Dependence of Ri_s on S^* and Re_λ

Another Reynolds number effect manifests itself when the cases having stationary levels of turbulence are compared. In general, we can characterize the state of the flow, in a coarse sense, by whether the turbulent kinetic energy is growing, decaying, or remaining unchanged (at equilibrium). Using the kinetic energy equation

$$\frac{\mathrm{d}K}{\mathrm{d}t} = P - \epsilon - B, \tag{10}$$

where P represents the shear production, ϵ the dissipation, and B the buoyant transfer of kinetic energy to potential energy, we can identify growing turbulence as cases where $\mathrm{d}K/\mathrm{d}t > 0$, decaying turbulence as having $\mathrm{d}K/\mathrm{d}t < 0$, and stationary turbulence as characterized by $\mathrm{d}K/\mathrm{d}t = 0$. Quantities used to assess the stationarity of the turbulence are the forcing parameter F, used by HKF:

$$F = \frac{P - B}{\epsilon} = \frac{1}{\epsilon}\frac{\mathrm{d}K}{\mathrm{d}t} + 1, \tag{11}$$

and the non-dimensional growth rate γ of JSV:

$$\gamma = \frac{1}{SK}\frac{\mathrm{d}K}{\mathrm{d}t} = -2b_{13}\left(1 - \frac{\epsilon}{P} - \frac{B}{P}\right). \tag{12}$$

Both F and γ measure the time rate of change of turbulent kinetic energy K.

Table 2 is a list of the stationary turbulence runs, cases in which the turbulence reaches an equilibrium state. As shown in HKF and JSV, in these stationary cases both the kinetic energy and the length scales become independent of time. The stationary Richardson number Ri_s associated with a given set of initial values of Re_λ, S^*, and energy spectrum is determined by varying Ri until the turbulence is found to be stationary using the above-described criteria. Further, the energy spectra for different non-dimensional times shown in figure 2 verify that the flow case shown

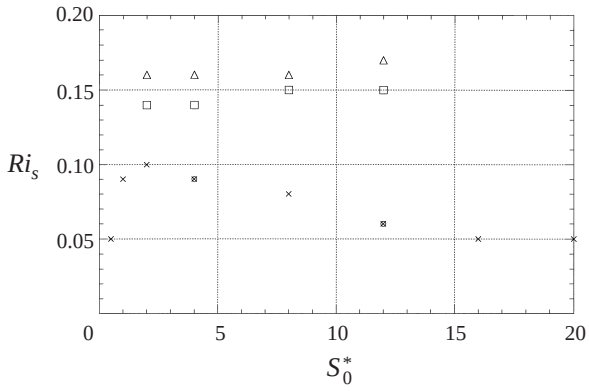

FIGURE 8. Ri_s vs. S_0^*. Data taken from the stationary turbulence runs with k^2-exponential initial energy spectra listed in table 2 and from JSV figure 18(*b*). ○, $Re_{\lambda,initial} = 22.36$; □, $Re_{\lambda,initial} = 44.72$; △, $Re_{\lambda,initial} = 89.44$; ×, JSV data.

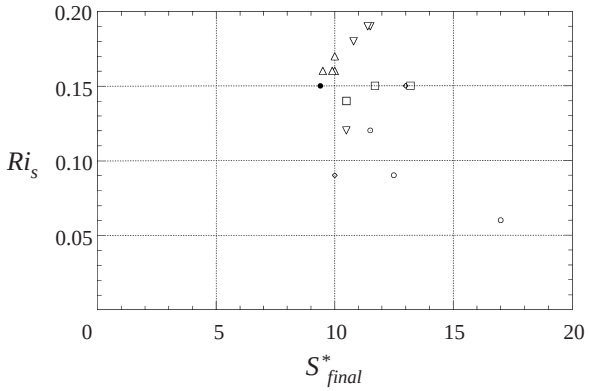

FIGURE 9. Ri_s vs. S^*_{final}. Data taken from the stationary turbulence runs listed in table 2. ○, $Re_{\lambda,initial} = 22.36$; ⊙, $Re_{\lambda,initial} = 33.54$; □, $Re_{\lambda,initial} = 44.72$; ◇, $Re_{\lambda,initial} = 44.72$, top-hat initial energy spectrum; ●, $Re_{\lambda,initial} = 67.08$; △, $Re_{\lambda,initial} = 89.44$; ▽, $Re_{\lambda,initial} = 89.44$, top-hat initial energy spectrum.

($Re_{\lambda,initial} = 89.44$, $Ri = 0.16$, $S_0^* = 2$) is indeed stationary, as evinced by the close resemblance of the developed spectra at $St = 8$ and 12.

Figure 8 shows the relation between the stationary Richardson number and the initial dimensionless shear rate S_0^*. As noted by JSV, at low Re_λ, Ri_s appears to have a peak as a function of S_0^*. While the initial value of S^* has a noticeable effect on Ri_s at low Reynolds number, at higher Reynolds numbers Ri_s is independent of the initial value of S^*. Again, it appears that more strongly turbulent flows either are insensitive to the effects of shear rate or develop a mechanism that counteracts the shear effects which does not occur in low-Reynolds-number flows. Plotting Ri_s versus the value of S^* at $St = 10$ (figure 9), on the other hand, reveals that the developed values of S^* vary only slightly among the stationary turbulence cases despite substantial changes in the initial conditions. (We take the values of the statistics at $St = 10$ to be the 'final' values, even though these may not be the fully converged values, because of the aforementioned questionable reliability of the code at large non-dimensional times.) The data point in figure 9 that is the most extreme outlier from the otherwise very narrow band of final shear numbers is from a low-Reynolds-number run. Given these

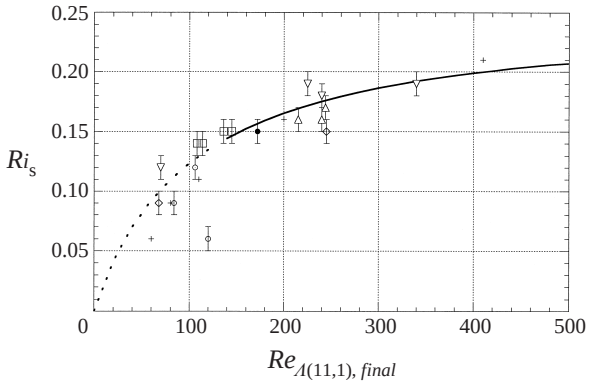

FIGURE 10. Ri_s vs. $Re_{\Lambda_{11,1},final}$. Data taken from the stationary turbulence runs listed in table 2 and HKF figure 6. Uncertainty of ± 0.01 shown. ○, $Re_{\lambda,initial} = 22.36$; ⊙, $Re_{\lambda,initial} = 33.54$; □, $Re_{\lambda,initial} = 44.72$; ◇, $Re_{\lambda,initial} = 44.72$, top-hat initial energy spectrum; ●, $Re_{\lambda,initial} = 67.08$; △, $Re_{\lambda,initial} = 89.44$; ▽, $Re_{\lambda,initial} = 89.44$, top-hat initial energy spectrum; +, HKF data; —, curve fit: $Ri_s = 0.25/(1 + 103/Re_{\lambda_{11,1}})$; – –, curve fit projected through the low-Reynolds-number data.

findings, it is clear that S^* does not play much of a role in determining the stationary Richardson number at high Reynolds number.

HKF suggest that for large enough initial Re_λ, Ri_s is a function of the instantaneous $Re_{\Lambda_{11,1}}$ only, where $Re_{\Lambda_{11,1}} = q\Lambda_{11,1}/\nu$ is a Reynolds number based on $\Lambda_{11,1}$, the integral length scale in the streamwise direction. The integral length scale is formally defined as

$$\Lambda_{ij,\alpha} = \frac{1}{R_{ij}} \int Q_{ij}(r_\alpha) \mathrm{d}r_\alpha, \tag{13}$$

where $Q_{ij}(r_\alpha)$ is the one-dimensional, two-point velocity correlation. (Other Reynolds numbers could be used without changing the qualitative nature of the results.) In figure 10 Ri_s is plotted versus $Re_{\Lambda_{11,1}}$ for all the conditions shown in table 2; the data in figure 6 of HKF are also shown. The uncertainty of ± 0.01 in the value of the stationary Richardson number arises from the fact that the stationary case was found iteratively, by adjusting Ri in increments of 0.01 until we found the value associated with an unchanging turbulent kinetic energy evolution profile, as denoted by a forcing parameter $F \approx 1$ or, equivalently, a non-dimensional growth rate $\gamma \approx 0$. While there is some scatter in the plot, the assumption that Ri_s depends only on $Re_{\Lambda_{11,1}}$ at higher Re appears nevertheless to be appropriate over both a broad range of S_0^* and a variety of initial energy spectra. Thus, figure 10 emphasizes the independence of Ri_s from S_0^* at high Reynolds number suggested by figure 8. HKF fit a curve $Ri_s = c_1/(1 + c_2/Re)$, where c_1 and c_2 are constants, to their data. Doing the same for the data in figure 10 yields a Pearson's R^2 of 0.61 with $c_1 = 0.25$ and $c_2 = 103$. This functional relation is especially appealing because it implies that Ri_s asymptotes to 0.25 for high Re, the value estimated by Miles (1961). However, this agreement may just be a coincidence, since Miles considered an infinitesimal disturbance to an inviscid stratified flow, and this flow contains both viscous effects and finite disturbances.

From these findings, three Reynolds number regions can be identified. At low Reynolds number ($Re_\lambda = 22.36$), S^* depends on its initial value, and Ri_s is a function of both the dimensionless shear rate and Reynolds number. At higher Reynolds number, S^* tends to a constant, and Ri_s is a function of Reynolds number only. At very high Reynolds number, S^* is again constant, and Ri_s also approaches a constant

value independent of Reynolds number. These regions are discernable in figure 10. At low Reynolds numbers ($Re_{\Lambda_{11,1}} < 150$), there is a fair amount of deviation in the value of the stationary Richardson number from the curve fit. The scatter reflects the dependence of Ri_s on other quantities, most notably S^*, in this range of Reynolds numbers. As the Reynolds number increases, the variability decreases, since the Ri_s dependence on S^* is declining. The very high-Reynolds-number region is not represented in figure 10, since none of our runs resulted in a high enough value of the final $Re_{\Lambda_{11,1}}$. Nevertheless, the asymptotic nature of the curve fit indicates that such a region does exist.

5. Scaling

Two approaches to scaling the results from our simulations are taken. The first is a Reynolds number approach derived from a result of JSV and intended as a means of scaling the stationary Richardson number of a flow. The second is based on the turbulent Froude number, as proposed by Ivey & Imberger (1991), and is intended as a means of scaling the final dimensionless shear rate of a flow. Each is presented in turn.

5.1. *Reynolds-number scaling*

JSV found that for low Reynolds number

$$Ri_s = \frac{1}{a}\frac{\lambda}{5l} Re_\lambda \frac{2}{S^*}\left(b - \frac{2}{S^*}\right) \tag{14}$$

and for high Reynolds number

$$Ri_s = \frac{1}{a}\frac{2}{S^*}\left(b - \frac{2}{S^*}\right) \tag{15}$$

where

$$a = 4\frac{\overline{\rho w}}{\rho w}\frac{w}{q}\frac{L_E}{l} \tag{16}$$

and

$$b = -2b_{13} \approx \text{constant}. \tag{17}$$

$L_E = \rho/S_\rho$ is the Ellison length scale, and l is the integral length scale.

Considering that the final value of S^* has just been shown to be a constant at high Reynolds numbers, equation (15) implies that the stationary Richardson numbers for these cases would be a constant if, as JSV assumed, a is constant. However, figure 11 shows that the coefficient a varies substantially with $Re_{\Lambda_{11,1}}$. Furthermore, figure 10 clearly indicates that Ri_s varies as a function of $Re_{\Lambda_{11,1}}$. If we let $l = \Lambda_{11,1}$, we can rewrite equation (16) as

$$a = 4R_{\rho w}\frac{wL_E}{\nu}\frac{1}{Re_{\Lambda_{11,1}}}, \tag{18}$$

where $R_{\rho w} = \overline{\rho w}/\rho w$ is the correlation coefficient for density and vertical velocity. Then, substituting this modified definition of a into equation (15), we arrive at

$$Ri_s = \frac{1}{4R_{\rho w}}\frac{\nu}{wL_E} Re_{\Lambda_{11,1}}\frac{2}{S^*}\left(b - \frac{2}{S^*}\right). \tag{19}$$

At high Reynolds number ($Re_{\Lambda_{11,1}} > 150$), $R_{\rho w}$ is constant with a value of 0.3,

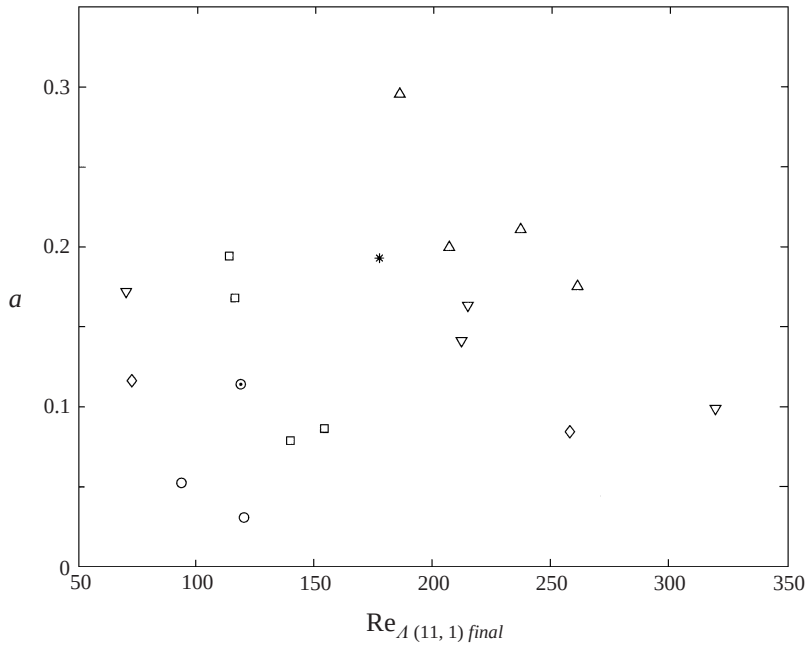

FIGURE 11. a vs. $Re_{\Lambda_{11,1},final}$. Data taken from the stationary turbulence runs listed in table 2. ○, $Re_{\lambda,initial} = 22.36$; ⊙, $Re_{\lambda,initial} = 33.54$; □, $Re_{\lambda,initial} = 44.72$; ◇, $Re_{\lambda,initial} = 44.72$, top-hat initial energy spectrum; ∗, $Re_{\lambda,initial} = 67.08$; △, $Re_{\lambda,initial} = 89.44$; ▽, $Re_{\lambda,initial} = 89.44$, top-hat initial energy spectrum.

and b_{13}, and therefore b, are also constant, and are approximately equal to -0.12 (see figure 4*a*). It has been established that S^* tends to a constant as Reynolds number increases. The quantity v/wL_E is an inverse turbulent Reynolds number based on vertical velocity fluctuations. From figure 12, a linear relation between the two Reynolds numbers seems reasonable; the data points which are the most significant outliers are from top-hat initial energy spectrum runs. Thus, at high Reynolds number, all the quantities on the right-hand side of equation (19) are either constant or can be expressed solely as functions of $Re_{\Lambda_{11,1}}$. It follows then that when it is large, the Reynolds number $Re_{\Lambda_{11,1}}$ is the dominant quantity in determining the stationary Richardson number, a conclusion which agrees with the findings of HKF. More quantitatively, assuming a functional form of

$$\frac{wL_E}{v} = m_1 Re_{\Lambda_{11,1}} + m_2 \tag{20}$$

causes equation (19) to become

$$Ri_s = \frac{c_1}{1 + c_2/Re_{\Lambda_{11,1}}}, \tag{21}$$

which is the same form as the curve fit in figure 10. It is important to emphasize that this scaling applies *only* to higher Reynolds numbers. At low Reynolds number, S^* depends on the initial conditions; similarly, b_{13} and $R_{\rho w}$ are not constant at low Re_λ. The variation in these parameters means that the simplification of equation (19) cannot be applied at low Reynolds numbers. It is therefore difficult to derive an expression for the stationary Richardson number valid at all Reynolds numbers. The curve fit in figure 10 was therefore applied only to the data for $Re_{\Lambda_{11,1}} > 150$.

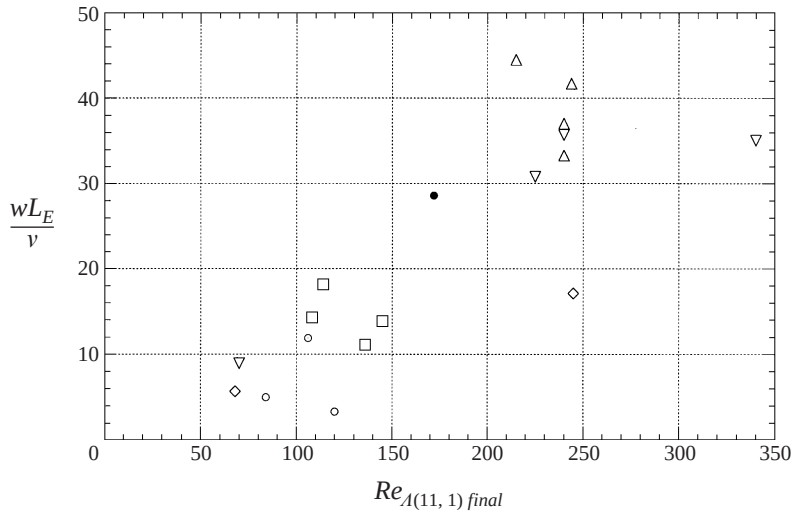

FIGURE 12. wL_E/v vs. $Re_{A_{11,1},final}$. Data taken from the stationary turbulence runs listed in table 2. ○, $Re_{\lambda,initial} = 22.36$; ⊙, $Re_{\lambda,initial} = 33.54$; □, $Re_{\lambda,initial} = 44.72$; ◇, $Re_{\lambda,initial} = 44.72$, top-hat initial energy spectrum; ●, $Re_{\lambda,initial} = 67.08$; △, $Re_{\lambda,initial} = 89.44$; ▽, $Re_{\lambda,initial} = 89.44$, top-hat initial energy spectrum.

5.2. *Froude-number scaling*

The difference in behaviour of the dimensionless shear number between the high and low initial Reynolds number cases becomes more understandable when the final state of the turbulence is examined from a different perspective. The turbulent Froude number Fr_t can be defined, following Ivey & Imberger (1991) and Briggs *et al.* (1998), as a ratio of length scales,

$$Fr_t = \left(\frac{L_O}{L_E}\right)^{2/3}, \tag{22}$$

where $L_O = (\epsilon/N^3)^{1/2}$ is the Ozmidov, or buoyancy, length scale and L_E is the Ellison, or turbulence, length scale. The Froude number is also commonly expressed as the ratio of time scales (see Ivey & Imberger 1991); we find the various alternatives to be qualitatively interchangeable. As noted in the introduction, since Fr_t is based on local turbulence quantities, it is a better parameter for the local characterization of turbulence than the gradient Richardson number, which is based on global quantities. The plots of the evolution of Fr_t show that, while all the varied initial S^* cases for high initial Re_λ (figure 13*a*) share a final turbulent Froude number, each of the low initial Re_λ (figure 13*b*) runs has a different final Fr_t. Characterizing the turbulence using the gradient Richardson number fails to reveal this fundamental difference between the high- and the low-Reynolds-number cases. The Froude-number-based analysis clearly shows that the low-Reynolds-number runs evolve dissimilarly, and thus there is no reason to expect any of the turbulent quantities in these cases to converge to a unique value. Here we, like Kaltenbach *et al.* (1994), find that what appears to be a dependence on Reynolds number can perhaps be better described as a Froude number effect.

If the turbulent Froude number parameterizes stratification effects better than the gradient Richardson number, it seems wise to investigate its role in stationary turbulence. Using the standard expressions for the production and buoyancy terms,

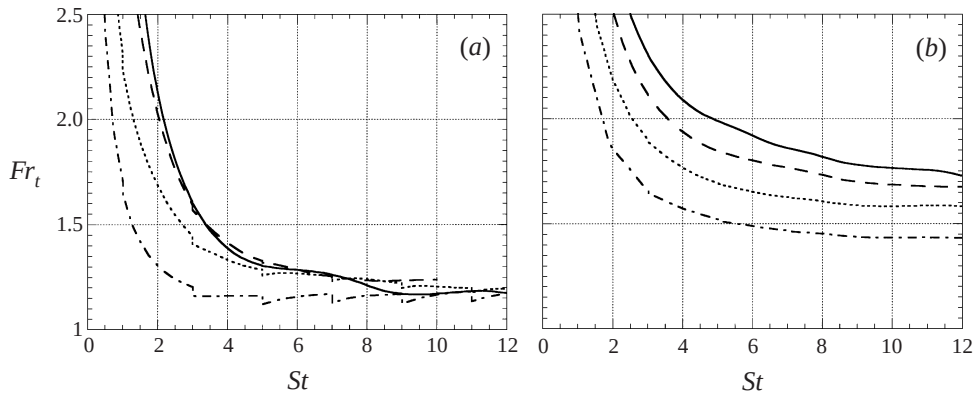

FIGURE 13. Evolution of the turbulent Froude number for various initial dimensionless shear rates. (*a*) $Re_{\lambda,initial} = 89.44$, $Ri = 0.16$; (*b*) $Re_{\lambda,initial} = 22.36$, $Ri = 0.06$. —, $S_0^* = 2$; – –, $S_0^* = 4$; · · · · ·, $S_0^* = 8$; · — ·, $S_0^* = 16$.

the kinetic energy equation given by equation (10) becomes

$$\frac{1}{2}\frac{\mathrm{d}q^2}{\mathrm{d}t} = -\overline{uw}S - \epsilon - \frac{g}{\bar{\rho}}\overline{\rho w}. \tag{23}$$

We designate α to be the growth rate of kinetic energy so that

$$\frac{1}{q^2}\frac{\mathrm{d}q^2}{\mathrm{d}t} = \alpha. \tag{24}$$

Note that this is simply the dimensional form of the growth rate given in equation (12), with $\alpha = \gamma S$. Using the definitions of the density–vertical-velocity correlation coefficient, the Brunt–Väisälä frequency, and the buoyancy length scale $L_b = w/N$, we find that the buoyancy term can be rewritten as

$$B = R_{\rho w} N^3 L_E L_b. \tag{25}$$

Since the buoyancy and Ozmidov scales are approximately equivalent (Itsweire *et al.* 1990, 1993), the definition of Fr_t given in equation (22) can be employed to introduce the turbulent Froude number into the scaling. Substituting the above expressions into the kinetic energy equation and recalling that $\overline{uw}$ can be written as $b_{13}q^2$ yields the following expression for growth rate:

$$\frac{1}{2}\frac{\alpha}{S} = -b_{13}\left[1 + \frac{1}{b_{13}S^*}\left(1 + \frac{R_{\rho w}}{Fr_t^{3/2}}\right)\right]. \tag{26}$$

For stationary flow, there is no growth or decay of kinetic energy, so that $\alpha = 0$. Applying the condition for stationary flow to equation (26), we can write an equation that predicts the value of S^* under stationary flow conditions:

$$S_s^* = -\frac{1}{b_{13}}\left(1 + \frac{R_{\rho w}}{Fr_t^{3/2}}\right). \tag{27}$$

Using values of b_{13}, $R_{\rho w}$, and Fr_t computed during the various flow simulations, we can estimate the values of S^* and compare these to the actual values of S^*, which are also computed as part of the turbulence statistics. Figure 14(*a*) shows that this relation does a reasonably good job of predicting S^*, regardless of initial Re_λ. Indeed,

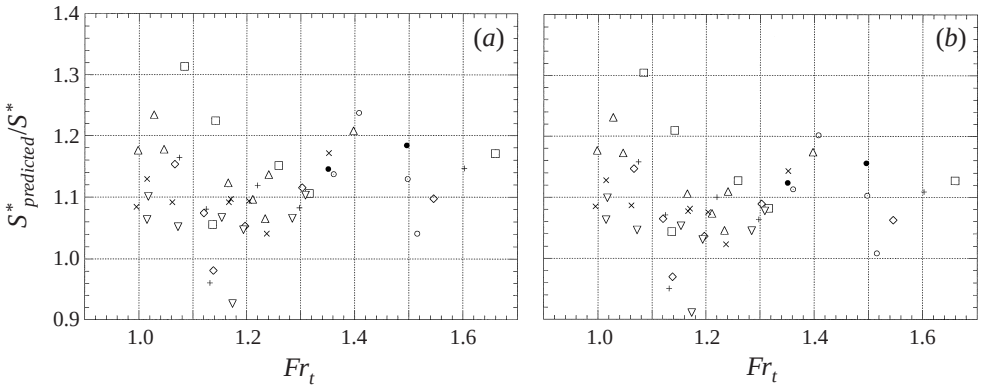

FIGURE 14. The ratio of predicted S^* to S^* vs. Fr_t for the stationary turbulence runs listed in table 2, at various St. (*a*) S^* predicted using equation (27). (*b*) S^* predicted using equation (30). ○, $Re_{\lambda,initial} = 22.36$ at $St = 8$; ⊙, $Re_{\lambda,initial} = 22.36$ at $St = 10$; ●, $Re_{\lambda,initial} = 22.36$ at $St = 12$; □, $Re_{\lambda,initial} = 44.72$ at $St = 8$; +, $Re_{\lambda,initial} = 44.72$ at $St = 10$; ◇, $Re_{\lambda,initial} = 44.72$ at $St = 12$; △, $Re_{\lambda,initial} = 89.44$ at $St = 8$; ×, $Re_{\lambda,initial} = 89.44$ at $St = 10$; ▽, $Re_{\lambda,initial} = 89.44$ at $St = 12$.

this scaling indicates that S^* can be predicted independently of Reynolds number. The fact that the ratio of predicted S^* to actual S^* tends to be greater than one suggests that the above scaling argument is off by a factor of a constant. The significance of the viability of this predictive scaling of S^* lies not in the importance of S^* itself as a parameter of modelling interest but rather in the fact that S^* is one of many quantities that reflects the state of the flow.

Alternatively, Ivey & Imberger (1991) defined the flux Richardson number as

$$Ri_f = \frac{B}{B+\epsilon} = \frac{1}{1+Fr_t^2/R_{\rho w}}. \tag{28}$$

The kinetic energy equation given by equation (10) can then be written

$$\frac{1}{2}\frac{\alpha}{S} = -b_{13} - \frac{1}{S^*}\frac{1}{1-Ri_f}. \tag{29}$$

For stationary flow, we then predict

$$S_s^* = -\frac{1}{b_{13}}\left(\frac{R_{\rho w}}{Fr_t^2}+1\right). \tag{30}$$

Figure 14(*b*) demonstrates that this scaling also accurately predicts the value of S^* for stationary turbulence. The only difference between equation (27) and equation (30) is the power of the turbulent Froude number. This difference originates from the difference in the approximations of w used in each scaling. By assuming that $L_O \sim L_b$, equation (27) assumes $w \sim (\epsilon/N)^{1/2}$, while the Ri_f fit of Ivey & Imberger assumes $w \sim (\epsilon L)^{1/3}$.

6. Conclusions

We have verified findings of JSV, namely that at low Reynolds number, the stationary Richardson number depends on both the Reynolds number and the dimensionless shear number. At higher Reynolds number, however, we established that the dimensionless shear number evolves to a constant regardless of its initial value and that

the stationary Richardson number varies only with Reynolds number. In so doing, we elucidated the importance of employing instantaneous quantities rather than the initial values of flow parameters. Examining the dissipation spectra, we hypothesize that a physical cause of the convergence of S^* to approximately 11 may be the increased dissipation of energy that is possible with the longer, thinner eddies that are a result of the higher shear.

We investigated the physical cause of this Reynolds number effect and discovered that the final turbulent states vary with shear rate at low Reynolds number but not at high Reynolds number. This discovery highlights the importance of using the appropriate parameters for characterizing a flow. The turbulent Froude number, which is based on local turbulence quantities, provides a more enlightening description of stratification than the gradient Richardson number, which is based on global quantities that remain constant throughout the development of a flow. While it may be more convenient to have a single global parameter with which to characterize stratification for modelling purposes, a local temporally evolving parameter appears more useful for investigating the physical processes of a flow. It is likely, then, that a turbulent Richardson number, as distinct from the gradient Richardson number, would work equally as well to correlate stratified turbulence statistics since such a parameter is also a local turbulent property.

We have also developed a large database on homogeneous sheared stratified turbulence that can be utilized for obtaining information relating to modelling and for physical insight. These data can be obtained from the authors.

The authors wish to thank Drs David Briggs and Michael Rogers for their advice and assistance. L. H. S., J. R. K., and J. H. F. would like to acknowledge the support provided by Dr Lou Goodman at the Office of Naval Research under Grant No. N00014-92-J-1611. The authors also wish to thank the referees for their helpful comments and suggestions.

REFERENCES

Briggs, D. A., Ferziger, J. H., Koseff, J. R. & Monismith S. G. 1998 Turbulent mixing in a shear-free stably stratified two-layer fluid. *J. Fluid Mech.* **354**, 175–208.

Garg, R. 1996 Physics and modeling of stratified turbulent channel flows. PhD thesis, Department of Mechanical Engineering, Stanford University.

Gerz, T., Schumann, U. & Elghobashi, S. E. 1989 Direct numerical simulation of stratified homogeneous turbulent shear flows. *J. Fluid Mech.* **200**, 563–594.

Holt, S. E. 1990 The evolution and structure of homogeneous stably stratified sheared turbulence. PhD thesis, Department of Civil Engineering, Stanford University.

Holt, S. E., Koseff, J. R. & Ferziger, J. H. 1992 A numerical study of the evolution and structure of homogeneous stably stratified sheared turbulence. *J. Fluid Mech.* **237**, 499–539 (referred to herein as HKF).

Itsweire, E. C., Holt, S. E., Koseff, J. R. & Ferziger, J. H. 1990 Direct numerical simulations of stably-stratified sheared turbulence: Implications for oceanic mixing. *Center for Turbulence Research Proceedings of the Summer Program*, pp. 163–180.

Itsweire, E. C., Koseff, J. R., Briggs, D. A. & Ferziger, J. H. 1993 Turbulence in stratified shear flows: Implications for interpreting shear-induced mixing in the ocean. *J. Phys. Oceanogr.* **23**, 1508–1522.

Ivey, G. N. & Imberger, J. 1991 On the nature of turbulence in a stratified fluid, part I: the energetics of mixing. *J. Phys. Oceanogr.* **21**, 650–658.

Jacobitz, F. G., Sarkar, S. & Van Atta, C. W. 1997 Direct numerical simulations of the turbulence evolution in a uniformly sheared and stably stratified flow. *J. Fluid Mech.* **342**, 231–261 (referred to herein as JSV).

Kaltenbach, H.-J., Gerz, T. & Schumann, U. 1994 Large-eddy simulation of homogeneous turbulence and diffusion in stably stratified shear flow. *J. Fluid Mech.* **280**, 1–40.

Lee, M. J., Kim, J. & Moin, P. 1990 Structure of turbulence at high shear rate. *J. Fluid Mech.* **216**, 561–583.

Miles, J. W. 1961 On the stability of heterogeneous shear flows. *J. Fluid Mech.* **10**, 496–508.

Piccirillo, P. S. & Van Atta, C. W. 1997 The evolution of a uniformly sheared thermally stratified turbulent flow. *J. Fluid Mech.* **334**, 61–86.

Rogallo, R. S. 1981 Numerical experiments in homogeneous turbulence. *NASA Tech. Memo*. 81315.

Rohr, J. J., Itsweire, E. C., Helland, K. N. & Van Atta, C. W. 1988 Growth and decay of turbulence in a stably stratified shear flow. *J. Fluid Mech.* **195**, 77–111.

Rogers, M. M. 1986 The structure and modeling of the hydrodynamic and passive, scalar fields in homogeneous turbulent shear flow. PhD thesis, Department of Mechanical Engineering, Stanford University.

Speziale, C. G., Gatski, T. B. & Sarkar, S. 1992 On testing models for the pressure-strain correlation of turbulence using direct simulations. *Phys. Fluids* A **4**, 2887–2899.

Speziale, C. G. & Mac Giolla Mhuiris, N. 1989 On the prediction of equilibrium states in homogeneous turbulence. *J. Fluid Mech.* **209**, 591–615.

Webster, C. A. G. 1964 An experimental study of turbulence in a density-stratified shear flow. *J. Fluid Mech.* **19**, 221–245.